Monitoring of in-situ chemical oxidation for remediation of dieselcontaminated soil with electrical resistivity tomography

Authors:

Teng Xia¹, Min Ma¹, Johan Alexander Huisman², Chuanpeng Zheng¹, Cuiling Gao³,

Deqiang Mao^{1*}

*Corresponding author

Affiliations:

¹School of Civil Engineering, Shandong University, Jinan 250061, China
² Institute of Bio- and Geosciences, Agrosphere (IBG-3), Forschungszentrum Jülich
GmbH, Germany

³Shandong Institute for Production Quality Inspection, Jinan, 250102, China

Emails:

Tengxiasdu@163.com, mamin_1122@163.com, s.huisman@fz-juelich.de,
zhengchuanpeng1127@163.com,124486040@qq.com, maodeqiang@sdu.edu.cn.

PostPrint for Self-archiving. Full publication is:

Xia, T., M. Ma, J.A. Huisman, C. Zheng, C. Gao, and D. Mao. 2023. Monitoring of insitu chemical oxidation for remediation of diesel-contaminated soil with electrical resistivity tomography. Journal of Contaminant Hydrology, 256, 104170.

Abstract

In-situ chemical oxidation (ISCO) with persulfate, an electrically conductive oxidant, provides a powerful signal for noninvasive geophysical techniques to characterize the remediation process of hydrocarbon contaminants. In this study, remediation with ISCO is conducted in laboratory sandboxes to evaluate the ability of electrical resistivity tomography (ERT) for monitoring the base-activated persulfate remediation process of diesel-contaminated soil. It was found that the resistivity of contaminated sand significantly decreased from 846 Ω ·m to below 10 Ω ·m after persulfate injection, and all measured chemical parameters showed a noticeable increase. Natural degradation and contamination plume migration were not evident in a reference sandbox without treatment. The area with a resistivity ratio < 0.95 based on imaging before and after injection indicated downward migration of the oxidation plume due to density-driven flow. A comparison between remediation and reference sandboxes showed that the observed resistivity decrease can be due to both contaminant degradation as well as the oxidation plume itself in the contaminated source zone. In contrast, the resistivity decrease in the area with low contamination concentration is attributed to the oxidation plume alone. The derived relationships between resistivity and contaminant indicators further emphasize that the contribution of contaminant consumption to resistivity change in the source area is 25.6%, while it is less than 16% in the low or non-contaminated area. Although this study showed that resistivity is not solely affected by the chemical transformation of diesel components, it can be combined with sampling data to allow an assessment of the effectiveness of ISCO

treatment and to identify target areas for subsequent treatment.

Keywords: ISCO, persulfate, electrical resistivity tomography, diesel contamination

1. Introduction

Hydrocarbon contamination of soil and groundwater represents a threat to the environment and human health. The presence of these compounds, e.g., gasoline, diesel or lubricants, in the environment may be associated with a variety of anthropogenic activities, such as oil extraction, leaks from storage tanks or pipelines, as well as smelting and oily wastewater discharge (Pinedo et al., 2013). Besides natural attenuation of contaminants (Serrano et al., 2008), various technologies, such as bioremediation (Imron et al., 2020), surfactant flushing (Karthick et al., 2019), and redox degradation (Flores Orozco et al., 2018), have been used to remediate soil or groundwater contaminated with hydrocarbons.

In-situ chemical oxidation (ISCO) is a soil remediation technique that is highly effective in removing contaminants, such as petroleum and halogenated hydrocarbons (Huling and Pivetz, 2006). Persulfate (S₂O₈²-) is a powerful oxidant with a redox potential (E⁰) of 2.01 V and is more persistent within soil than many other ISCO oxidants (Yen et al., 2011). In addition, persulfate can be activated to further increase its reactivity. Activation can be achieved by four main methods relying on the addition of hydrogen peroxide, ferrous or chelated iron, heat, or bases to achieve a high pH (Huling and Pivetz, 2006). In particular, base activation (high pH) of persulfate has been applied in around 60% of the ISCO remediation studies with persulfate (Furman et al., 2010). After base activation, powerful oxidants can be generated depending on the achieved pH, in particular sulfate (SO₄*, E⁰=2.6 V) and hydroxyl radicals (OH*,

E⁰=2.7 V) (Huling and Pivetz, 2006). These radicals with strong oxidizing properties can consume many petroleum contaminants, such as benzene and polyaromatic hydrocarbons. The implementation of ISCO remediation techniques at contaminated sites needs to be accompanied by real-time monitoring to capture the development of the chemical reaction characteristics of contaminants and oxidants for assessment purposes.

Accurate information about remediation progress is usually constrained by the lack of sampling density. The shortcomings of traditional monitoring methods have promoted the application of geophysical methods (Lekmine et al., 2017). The electrical resistivity method is the most commonly used geophysical technique in contaminant studies as the subsurface resistivity depends heavily on the effective porosity, saturation and the conductivity of the pore water (Binley and Slater, 2020). Electrical resistivity tomography (ERT) is a non-destructive electrical imaging method that can be used from the surface as well as between boreholes to obtain valuable information about the distribution of the electrical properties of soils and aquifers. During resistivity measurements, current is injected using two electrodes, while the potential difference is measured at two other electrodes (Kemna et al., 2002). For a larger survey area, more electrodes are needed and multi-channel measurements (Dahlin and Zhou, 2006) make the ERT method faster and easier to perform in the field. ERT has been widely used in a range of near-surface applications, including monitoring of groundwater flow (Coscia et al., 2011), saline water intrusion (Alpaslan, 2021) as well as tracer tests (Müller et al., 2010).

Several studies have shown the potential of ERT measurements on sites contaminated with petroleum hydrocarbon (e.g. Sentenac et al., 2015). Time-lapse ERT imaging was found to be particularly powerful to monitor temporal changes in subsurface resistivity, which is commonly related to the variation of saturation (water and/or oil), temperature and pore fluid composition associated with migration, degradation, and remediation (Seferou et al., 2013). Both numerical and field tests have illustrated that cross-borehole surveys are best suited for reconstructing tracer paths and contaminant plumes (Lekmine et al., 2017). Several laboratory studies have established a relationship between resistivity and contaminant concentration by mixing different contents of petroleum hydrocarbon contamination with uncontaminated soil (e.g., Schmutz et al., 2010). For non-wetting oil, it was found that the measured resistivity correlates well with the hydrocarbon content, i.e. a higher content corresponds to a higher resistivity (Revil et al., 2011; Schwartz et al., 2012). Typically, laboratory as well as field studies using ERT monitoring of petroleum hydrocarbon contamination have focused on the migration of the contaminant plume (Halihan et al., 2017; Deng et al., 2017). Although previous studies have used electrical resistivity methods to monitor the remediation or degradation processes of petroleum hydrocarbons such as diesel (Mao et al., 2016), monitoring of persulfate remediation has mostly been based on periodic chemical sampling (He et al., 2022).

Within this context, the aim of the present work is to investigate the ability of ERT monitoring of the ISCO remediation process to evaluate the effectiveness of persulfate remediation in real time. Diesel was chosen as the hydrocarbon contaminant and the remediation process by base-activated persulfate was monitored using cross-borehole ERT measurements in laboratory experiments. Specifically, the relationship between diesel content and resistivity is first verified by sand column measurements, and then two parallel sandbox experiments were conducted. For both remediation and reference sandbox tests, the resistivity changes of diesel contaminated soil were monitored together with hydrochemical indicators. Additionally, contaminant indicators of soil and water samples from the two sandboxes were measured after the monitoring experiments.

2. Materials and Methods

2.1 Experimental setup and materials

Two identical sandboxes were designed for monitoring experiments, i.e., a remediation sandbox with persulfate injection and a reference sandbox. The dimensions of both sandboxes are 51 cm high × 60 cm long × 10 cm thick (Fig. 1). Non-polarizing Ag-AgCl electrodes (4 mm in diameter) were fixed to the inner wall of the sandbox in 4 rows with 16 electrodes each (Fig. 1). The vertical spacing between electrodes was 2.7 cm, and the lowest electrode was located 3.8 cm above the bottom of the sandbox. Only the tip of each electrode was allowed to have contact with the porous media, and the remaining of the electrode was wrapped with insulated epoxy (Mao et al., 2015) to

mimic a point measurement to the extent possible.

Two measurement tubes were set up on both sides of the sandbox for hydrochemical monitoring during the experiment. The lower 8 cm segment was punched similar to a well screen to allow water sampling. The persulfate injection tube with a 5 mm inner diameter was located in the center of the remediation sandbox, and the lower 10 cm was punched with holes for persulfate outflow while the bottom of the tube was sealed to allow only horizontal flow. All these components were made of PMMA to minimize electrical disturbances. All experiments were performed at room temperature (25 \pm 2 °C).

Quartz sand with a median grain diameter of $d_{50} = 500 \pm 10$ µm, a porosity of 0.41 ± 0.02 and a bulk density of 5.076 g/cm³ was used for all experiments (China, Macklin Co., Ltd.). The difference between the column's unsaturated and saturated weight was used to determine its porosity, and the ratio of weight to volume was used to determine its bulk density. The maximum capillary rise of the quartz sand was 15 cm determined using the standpipe method. Before the experiments, the quartz sand was washed with distilled water and dried at 90 °C for 12 h. The sand was saturated with an NaCl electrolyte with an electrical conductivity of 45 mS/m. The chemical substances sodium persulfate (Na₂S₂O₈, Analytical Reagent/AR, 99.7% purity), sodium hydroxide (NaOH, AR) and sodium chloride (NaCl, AR) were acquired from Macklin Co., Ltd of Shanghai, China. Diesel fuel was purchased from the Chinese Petroleum Corporation, China, and

its composition and characteristics are similar to those of diesel fuel no.1 reported by Gad (2005). It is composed of about 75% saturated hydrocarbons, e.g., alkanes (C_nH_{2n+2}) , cycloalkanes (C_nH_{2n}) , and 25% aromatic hydrocarbons, e.g., mono-aromatic hydrocarbon (C_nH_{2n-6}) . The diesel used in the experiments has a density between 0.82 and 0.86 g/ml. Typical atomic mass concentrations are approximately 86% C, 14% H and a small amount of sulfur, depending on the crude oil source and cleaning quality. Accordingly, the average chemical formula for diesel ranges from about $C_{10}H_{20}$ to $C_{15}H_{28}$.

2.2 Column experiments

Bulk electrical conductivity of porous media can be influenced by both surface conductivity and pore fluid conductivity, and these two contributions cannot easily be separated in resistivity measurements (Lesmes and Frye, 2001). Therefore, additional column experiments were conducted to separate the effects of surface conductivity and diesel content. For this, laboratory columns similar to those reported by Mellage et al. (2018) were used. The Ontash PSIP instrument (www.ontash.com) was used for complex resistivity measurements using a four-electrode configuration. Resistivity magnitude $|\rho| = 1/|\sigma|$ (in Ω ·m) and phase shift ($-\phi$) (in mrad) were measured at 19 log frequency intervals between 0.001 and 1000 Hz.

Four different diesel concentrations were used, i.e., 0.0 g/kg, 10.6 g/kg, 63.5 g/kg and 105.9 g/kg. Based on the proportions of diesel and electrolyte, the desired oil and water

saturations were obtained and the content of diesel in the sand was calculated, while the porosity was assumed to be constant. This resulted in a water saturation of 1.00, 0.95, 0.70 and 0.50 for the four different diesel concentrations. Note that the electrolyte was added to sand first and diesel was then added, which was consistent with the procedure for the preparation of samples with non-wetting oil reported by Revil et al. (2011). Following the mixing, we packed the mixture tightly in the column. Similar packing procedures can be found in previous studies (e.g., Schwartz et al., 2012). After all columns were measured, about 5 pore volumes of base-activated persulfate solution consisting of 3 M sodium hydroxide and 0.5 M persulfate was injected into the sand column with a diesel content of 105.9 g/kg using a peristaltic pump, and the complex resistivity response was measured again.

2.3 Diesel contaminated sand and base-activated persulfate remediation

Diesel was selected as the contaminant in this study are due to its low toxicity, relatively low volatility, and its similar electrical characteristics to other hydrocarbons. The diesel-contaminated sand used in the sandbox experiments was prepared in the same way as in the column experiments using a diesel content of 105.9 g/kg. The pore space was fully saturated with NaCl electrolyte for uncontaminated sand. Similar to the packing method in the column experiments, the sand was put into the sandbox after saturation and was manually compressed by a rectangular plate during the packing process. The boundaries between contaminated and uncontaminated sand were stabilized by two thin plates during sample preparation, which were removed after

packing. The contaminated sand was packed in the middle of the sandboxes (x=26-34 cm, z=20-42 cm) (Fig. 1a). The whole packing process was completed within 40 min. The filling height of the sand was 50 cm, and the water level in the monitoring tubes on both sides was 25.5 cm. Thus, we assumed that the initial saturation height was 40.5 cm (water level height of 25.5 cm and 15 cm capillary rise). To minimize evaporation, the top layer of sand was covered with a 1 cm thick layer of silt and the surface was covered with plastic wrap.

Sodium hydroxide was used to activate the persulfate. The radicals generated in the base-activated persulfate system are sulfate (SO₄*-), hydroxyl (OH*) and superoxide radicals (O₂*-, E⁰=0.33 V) (Watts, 2011; Liang and Guo, 2012). The alkaline pH environment promotes the following activating reactions:

$$Na_2S_2O_8 + H_2O \rightarrow SO_5^{2-} + SO_4^{2-} + 2H^+,$$
 (1)

$$SO_5^{2-} + H_2O \xrightarrow{Base} HO_2^{-} + SO_4^{2-} + H^+,$$
 (2)

$$S_2O_8^{2-} + HO_2^{-} \rightarrow SO_4^{--} + SO_4^{2-} + H^+ + O_2^{--}.$$
 (3)

The net reaction of base-activated persulfate decomposition is summarized as (Furman et al., 2010):

$$2S_2O_8^{2-} + 2H_2O \rightarrow 3SO_4^{2-} + SO_4^{-} + O_2^{-} + 4H^+. \tag{4}$$

In conditions with pH > 10, formation of SO₄ may promote the formation of OH, initiating a series of radical propagation and termination chain reactions in which organic compounds can be transformed (Liang and Lee, 2008):

$$SO_4^{\bullet-} + H_2O \rightarrow SO_4^{2-} + OH^{\bullet} + H^+,$$
 (5)

$$SO_4^{\bullet-} + OH^{-} \rightarrow SO_4^{2-} + OH^{\bullet}. \tag{6}$$

The simultaneous generation of SO₄, OH, and O₂ leads to the generation of molecular oxygen (Furman et al., 2010; Watts, 2011), i.e.,

$$OH' + O_2' \rightarrow O_2 + OH', \tag{7}$$

$$SO_4$$
 $\rightarrow O_2 + SO_4^2$. (8)

Thus superoxide (O2*) is reductive and may constrain the effects of hydroxyl (OH*) and sulfate radicals (SO4*). SO4* and OH* have been reported to play a dominant role in the degradation of diesel. Although sulfate radicals are highly oxidizing, they are more likely to react with short-chain aliphatic hydrocarbons and mono- or lower-cyclic aromatic hydrocarbons in diesel by hydrogen extraction (Eq. 9) or electron transfer (Eq. 10) to produce oxidized organic compounds (Waldemer et al., 2007; Zhao et al., 2013). In contrast, hydroxyl radicals can react with most components, including those that cannot be oxidized by sulfate radicals, thus contributing to the breaking of C=C bonds (Eq. 11) or extracting hydrogen from C-H bonds (Eq. 12). The resulting degradation reactions can be written as (Cronk 2008):

$$SO_4^- + RH \rightarrow R^+ + HSO_4^-, \tag{9}$$

$$SO_4^{\bullet} + RH \rightarrow RH^{\bullet} + HSO_4^{\bullet},$$
 (10)

$$OH' + RH \rightarrow R' + H_2O, \tag{11}$$

$$OH' + RH \rightarrow RH_2O'. \tag{12}$$

where RH represents the organic carbon compounds, and R*, RH** and RH₂O* represent the oxidized organic compounds.

To investigate base-activated persulfate remediation of diesel-contaminated soil, 0.5 M sodium persulfate and 3 M sodium hydroxide (250 ml of each solution) were mixed and immediately injected into the remediation sandbox using a peristaltic pump (20 mL/min) on day 21 after sample preparation. The ratio of persulfate to sodium hydroxide was similar to Furman et al. (2010). The summary statistics of sandbox experiment are shown in Table 1.

2.4 Data acquisition and processing

Resistivity measurements were conducted seven times throughout the monitoring experiment, at day 11, 21, 38, 55, 115, 149 and 181. Measurements were collected in triplicates using a "skip-two" and "skip-four" measuring protocol (Slater et al. 2000). For each current electrode pairs AB, potential electrode pairs MN were selected with the same skip. For example, for the "skip-two" protocol, for AB = 1 and 4, potential electrode pairs MN = 5 and 8, 6 and 9, and so on were measured; while for the "skip-four" protocol, for AB = 1 and 6, MN = 7 and 12, 8 and 13, and so on were measured. In this way, the measurement array also contained reciprocal measurements, e.g., for AB = 1 and 4, MN = 5 and 8; while the corresponding reciprocal measurement array is AB = 5 and 8, MN = 1 and 4. Each between-borehole dataset contained 1112 measurements, e.g., 1112 measurements for electrodes 1-32, 17-48 and 33-64, respectively. Consequently, 3336 resistance data were measured to cover the whole sandbox. The resistivity measurements were made with the multi-channel ABEM Terrameter LS2 instrument (www.guidelinegeo.com). The acquisition time for all

dataset was 35 min. The inversion was performed using a 3D finite element code written in the *Comsol* and *Matlab* environments (Mao et al., 2015). We assumed no resistivity variation in the *y* direction due to the small sandbox thickness. Therefore, the inversion results are presented as 2D tomograms.

Besides geophysical measurements, chemical parameters were measured on the left and right sides of each sandbox. The interval during the first 40 days was 4 days, while the interval was increased to 15 days after 40 days due to insignificant changes in the measured chemical parameters. The investigated parameters included oxidationreduction potential (ORP), pH, dissolved oxygen (DO) and electrical conductivity. ORP, pH and DO were measured using a multi-parameter analyzer (Leici DZB-715, China), and electrical conductivity was measured using a conductivity meter (ECTestr 11+, USA). At the end of the experiment, eight positions in each sandbox (S1-S8 and S9-S16) were selected to collect soil samples. In addition, water samples (W1-W2 and W3-W4) were collected at the bottom of both sides of each sandbox using water outlet valves (Fig. 1a). The soil samples were analyzed for total organic carbon (TOC) and total petroleum hydrocarbons (TPH), while water samples were analyzed for petroleum, chemical oxygen demand (COD) and anion concentrations (SO₄²- and HCO₃-). The TOC in the soil samples was measured using a potassium dichromate oxidation spectrophotometric method and the TPH in these samples was determined using a gas chromatography method. The petroleum, COD, SO₄²⁻ and HCO₃⁻ concentration in the water samples were determined by infrared spectrophotometry, dichromate, ion

chromatography and titration methods, respectively. The selection of chemical parameters followed the *Geological survey and evaluation standards for soil and groundwater in contaminated sites* (China Geological Survey, 2014).

3. Results

3.1 Effect of diesel contamination on complex resistivity

The results of the column experiments indicate that the resistivity and the phase increase with diesel content (Fig. 2), i.e., the oil saturation. This is consistent with results described by Cassiani et al. (2009) and Schmutz et al. (2010) for non-wetting oil. The values of the resistivity magnitude and the phase peak are provided in Table 2. The resistivity increased from 82.6 Ω ·m for 0.0 g/kg diesel content (S_w = 1) to 745.2 Ω ·m for 105.9 g/kg diesel content (S_w = 0.5). The peak phase increased from 2.36 mrad for 0.0 g/kg diesel content to 6.6 mrad for 105.9 g/kg diesel content. Moreover, a shift in peak frequency from 0.022 Hz at 0.0 g/kg diesel to 0.0046 Hz at 105.9 g/kg diesel content was observed. These features are well-explained by the model developed by Schmutz et al. (2010).

After the injection of base-activated persulfate into the sand column with 105.9 g/kg diesel content, the resistivity decreased significantly from 745.2 Ω ·m to about 2.6 Ω ·m, while a phase measurement with sufficient accuracy could not be obtained. This is because the activated persulfate produces a large number of ions, and the resulting high salinity environment is not favorable for accurate complex resistivity measurements

(Xia et al., 2021; Niu et al., 2016).

The interpretation of ERT inversion results in contaminant studies is sometimes complicated by geological heterogeneity, which can produce resistivity differences that are stronger than those associated with the presence of the oil itself (Deng et al., 2017). To ensure sufficient contrast in this study, a high diesel content of 105.9 g/kg was used in the sandbox experiments. With this level of contamination, the resistivity of the contaminated sand is about 9 times higher than that of clean water-saturated sand.

3.2 Results of electrical resistivity tomography measurements on sandboxes

A total of seven resistivity measurements were taken over a six month period. The reciprocal errors of all datasets are summarized in Fig. 3. Reciprocal error refers to the relative error of data obtained from two sets of reciprocal measurements. The data quality obtained in the remediation sandbox is slightly worse than that of reference sandbox, which is particularly evident before and after persulfate injection. Specifically, the reciprocal errors is below 2% on day 11 before persulfate injection for 85.4% of the measurements, and this percentage is reduced to 80.8% on day 21 after persulfate injection. For the reference sandbox, the percentage of measurements with errors <2% is similar on day 11 and 21 (85.3% and 85.7%, respectively), which is also consistent with the percentage obtained before persulfate injection for the remediation sandbox. It is important to note that the overall data quality is generally acceptable (Loke et al., 2015), with at least 98.7% of reciprocal errors <5% for the reference sandbox and at

least 96.6% of reciprocal errors <5% for the remediation sandbox.

Time-lapse ERT inversion results are presented in Fig. 4. At the end of the monitoring experiment (day 181), the water level in the reference sandbox was 24.3 cm, and the water level in the remediation sandbox was slightly higher at 25.1 cm due to the persulfate injection. Therefore, the saturation heights (red dashed lines) were also slightly different with 39.3 cm for the reference sandbox and 40.1 cm for the remediation sandbox. Before persulfate injection, the resistivity distributions are similar for the remediation and reference sandbox. Specifically, the resistivity within the black rectangle ranges from 575 Ω ·m to 1200 Ω ·m with an average value of 846 Ω ·m, corresponding to the diesel contaminated sand, which is 150 Ω ·m higher than the surrounding resistivity.

After persulfate injection (day 21) in the remediation sandbox, the resistivity decreased significantly especially at the injection port where the resistivity reached values lower than $10~\Omega\cdot m$, which is consistent with the results of the sand column experiments. In addition, it was also observed that a low-resistivity plume migrated to the left and right side beyond the originally contaminated area immediately after injection. As time progressed, this plume was observed to gradually expand and migrate downwards from day 38 to 181. In addition, the resistivity of the unsaturated zone above 39 cm in the two sandboxes gradually increased, which is attributed to water evaporation over the experimental period.

The resistivity around the contaminated sand shows an increase in both vertical and horizontal directions at the end of the experiment in the reference sandbox. However, these increases are only minor suggesting that diesel migration is not significant. Sentenac et al. (2015) also reported limited migration of hydrocarbons in a similar sandbox experiment, also in the presence of a hydraulic gradient from left to right that may lead to diesel migration by advection. Therefore, the lack of migration in our experiments with diffusion-dominated diesel transport is not surprising. In addition, the gentle resistivity variation also indicates that the natural degradation of contaminated sand is not significant. Note that the high resistivity response of at the top of sandbox is not only caused by evaporation, but also may be caused by upward movement of free-phase diesel.

3.3 Chemical analysis and sampling results

ORP, pH, DO and conductivity are important indicators to characterize the oxidation reactions, and Fig. 5 shows their variation during the remediation and reference experiment. In general, all chemical parameters measured on day 21 in the remediation sandbox showed a noticeable jump due to the injection of persulfate, while the results for the reference sandbox showed a slight downward trend. Specifically, the ORP measured on day 21 in the remediation sandbox was 417 mV, which was higher than that measured in the reference sandbox (263 mV) saturated with NaCl electrolyte. These results are consistent with experiments conducted by Zhao et al. (2013), who

showed that the ORP of the base-activated persulfate reaction system (pH=12) in laboratory vials was 562±17 mV, while the background value without persulfate was 367 mV. The increased ORP reflects the oxidative properties of persulfate. With respect to pH, it is evident that highly alkaline conditions (pH>13) were created after base-activated persulfate injection. In these conditions, it is expected that superoxide (O₂*·), hydroxyl (OH*), and sulfate radicals (SO₄*·) were generated. At the same time, O₂*· radicals were likely scavenged by OH* radicals through the reaction given in Eq. (7). Similarly, SO₄*· radicals were removed through the reaction given in Eq. (8). This resulted in the generation of one mole of O₂ per mole of generated O₂*· (Furman et al., 2010; Hayyan et al., 2016). Additionally, persulfate dissolves in water and then reacts with water to produce a small amount of O₂, which is another reason for the increase in DO:

$$2Na_2S_2O_8 + 2H_2O \rightarrow 2Na^+ + 4SO_4^{2-} + 4H^+ + O_2. \tag{13}$$

Therefore, the DO measured in the remediation sandbox increased by approximately 38.5% after persulfate injection (~9.5 mg/L) compared to that measured before persulfate injection (~6.86 mg/L) and reference sandbox (~6.85 mg/L). In addition, consumption of hydroxide as well as the decomposition and activation of persulfate release hydrogen ions and other anions, e.g., SO₄²⁻, HCO₃⁻ or CO₃²⁻, which leads to a decrease of pH and an increase of conductivity (Huang et al., 2002; Li et al., 2020; Chang et al., 2022). At the same time, persulfate consumption results in a decrease of ORP and DO. Although the monitoring tubes are not located in the direct vicinity of the persulfate injection, the measured data still reflect the general chemical variations in

the sandboxes. It is anticipated that the changes in the chemical parameters near the injection tube will be even more dramatic. At the same time, the difference in position also explains why the change of chemical parameters is insignificant in the early stages and more evident in the later stages, i.e., it takes time for the plume to migrate to the water sampling ports.

The chemical parameters measured in soil and water samples at the end of the experiments are shown in Table 3 (see Fig. 1 for sampling points). The results of the soil samples suggest that the hydroxyl and sulfate radicals formed by base-activated persulfate resulted in substantial degradation of diesel, especially near the outflow holes. For example, the measured TOC and TPH at location S1 in the remediation sandbox is 1.73 g/kg and 1.67 g/kg, respectively. This was much lower than the concentrations measured at the same location S9 in the reference sandbox, where the TOC was 36.1 g/kg and the TPH was 33.8 g/kg. The degradation products are eventually mineralized and converted into CO₂ or metabolic byproducts (Arato, et al., 2014). For instance, the degradation reactions of benzene, a component of diesel, with SO₄- and OH are (Liu et al., 2016):

$$SO_4^{\bullet -} + C_6H_6 \rightarrow C_6H_6^{+\bullet} + SO_4^{2-},$$
 (14)

$$OH^{\bullet} + C_6H_6 \rightarrow C_6H_7O^{\bullet}.$$
 (15)

In addition, short-chain aliphatic hydrocarbons, e.g., decane, which are another major component of diesel, undergo hydrogen extraction from the C-H bonds when reacting with SO₄* and OH*:

$$SO_4^- + C_{10}H_{22} \rightarrow C_6H_{11}^+ + HSO_4^-,$$
 (16)

$$OH^{\bullet} + C_{10}H_{22} \rightarrow C_{10}H_{21}^{\bullet} + H_2O.$$
 (17)

The net chemical reactions in which benzene and decane are completely degraded by persulfate are:

$$15S_2O_8^{2-} + C_6H_6 + 12H_2O \rightarrow 6CO_2 + 30H^+ + 30SO_4^{2-}, \tag{18}$$

$$31S_2O_8^{2-} + C_{10}H_{22} + 20H_2O \rightarrow 10CO_2 + 62H^+ + 62SO_4^{2-}$$
. (19)

We assume that $C_{12}H_{23}$ is the average chemical formula for diesel, which does not contain structural information but only takes into account the carbon/hydrogen ratio (Gad, 2005), i.e., $C_{12}H_{23}$ does not refer to alkynes or alkenes alone, but is composed of various hydrocarbons. Accordingly, the net chemical reaction of diesel consumption by persulfate can be expressed as:

$$71S_2O_8^{2-} + 2C_{12}H_{23} + 48H_2O \rightarrow 24CO_2 + 142H^+ + 142SO_4^{2-}$$
. (20)

This net reaction is consistent with the observed chemical parameters. After degradation in the remediation sandbox, the TPH and TOC of the soil samples decreased compared to the reference sandbox, while the SO₄²⁻ and HCO₃⁻ concentrations in the water samples increased (Table 3). Considering that HCO₃⁻ was not present in the electrolyte used to prepare the sample, it is likely to be a degradation product from the oxidation of diesel (Wu, 2021). Accordingly, the degradation of diesel by persulfate releases a large number of ions, causing an increase in SO₄²⁻ and HCO₃⁻ concentrations measured at locations W1 and W2 compared to locations W3 and W4, e.g., the average concentration of SO₄²⁻ and HCO₃⁻ in water samples collected from the remediation sandbox are 3235 mg/L and 793 mg/L, while those measured in the reference sandbox are 14 mg/L and 204 mg/L. Although diesel is characterized by low

solubility, a small fraction of dissolved phase still is expected to occur in the saturated zone (Atekwana and Atekwana, 2010). The average values of the petroleum concentration and COD in the reference sandbox were 2.3 mg/L and 139.5 mg/L, which are higher than those measured in the remediation sandbox where dissolved diesel components were likely oxidated.

4. Discussion

4.1 Migration pathway of oxidation plume

Based on the column and sandbox experiments, it is evident that the persulfate remediation system causes a significant resistivity decrease. To better capture the observed changes in resistivity caused by the persulfate injection, resistivity ratio tomograms are presented in Fig. 6. The measurements before the injection (day 11) were used as a reference. Persulfate injection caused a decrease in resistivity in a significant part of the sandbox as indicated by the area with resistivity ratio < 1. Although the reciprocal error indicates that the quality of data acquisition is acceptable, we nevertheless prefer to take a conservative approach and assume that the area with a resistivity ratio less than 0.95 is affected by oxidation plume migration (blue solid lines).

Considering that the injection locations (20-30 cm) are distributed on the side walls of a tube sealed at the bottom, persulfate is expected to radially spread away from the injection tube at the center. Following the persulfate injection at day 21, the resistivity ratio near the outflow locations was less than 0.1 and the tomogram suggests that the

migration distance of persulfate in horizontal direction (x=16-44 cm) was larger than in the vertical direction (z=10-34 cm). Since persulfate has a high solubility in water (73 g/100 ml at 25 °C) and the density (e.g., 2.59 g/mL for sodium persulfate) at 25 °C is greater than water (Yen et al., 2011), persulfate solution with a high concentration can migrate due to density-driven transport (Huling and Pivetz, 2006). This is also observed in the remediation sandbox. After 17 days of persulfate injection (day 38), the oxidation plume has clearly migrated downward and it reached the bottom of the sandbox on day 115. Given the slow migration of the contaminant, it is clear from Eq. (1)-(6), (13) and (20) that the main components of this oxidation plume stem from the persulfate remediation system and ions released by the associated chemical reactions. In the later stages of the experiment after the plume reached the bottom of the sandbox (especially on day 149 and 181), the oxidation plume gradually migrated outward to both sides again under the influence of concentration differences. Although the lateral migration distance of persulfate during injection was greater than that in vertical direction due to the high injection pressure, the oxidation plume was dominated by vertical migration due to density-driven transport. The results clearly showed that this general migration pathway of the persulfate could easily be captured by the electrical resistivity distribution, which highlights the potential of time-lapse ERT images for capturing the delivery and fate of persulfate in ISCO remediation in field conditions. It should be noted that parts of unsaturated zone above 39 cm have a resistivity ratio greater than 1, indicating that the resistivity of this area has increased after injection compared with that before injection. Besides evaporation, considering that surface is covered with silt, the capillary rise phenomenon may drive a small amount of freephase diesel to migrate upward.

4.2 Influence of diesel degradation on the resistivity distribution

The resistivity monitoring results for the reference sandbox indicate that natural degradation and migration of the contaminated plume are limited during the entire experiment. To further illustrate this, the resistivity difference ($\rho_{reference}$ - $\rho_{remediation}$) between sandboxes is analyzed to characterize the resistivity response caused by persulfate remediation alone (Fig. 7). Clearly, the resistivity of the reference sandbox is higher than that of the remediation sandbox everywhere. Specifically, the results illustrate that the largest differences (>600 Ω ·m) correspond to the location of the outflow within the contaminated sand (white solid rectangle). At these locations, the average resistivity difference for the two sandboxes is about 1010 Ω ·m. Obviously, the resistivity difference within the contaminated sand is not only related to the change of diesel concentration, but also to the oxidation plume. The blue solid lines in Fig. 6 show the area of oxidation plume migration (z<34 cm) derived from a resistivity ratio <0.95 (see Fig. 6). At the same time, the red solid lines delineate the area below the height of plume migration with a resistivity difference above 80 Ω ·m. The average resistivity difference within the red solid lines (excluding the contaminated sand in the black rectangle) is 126.7 Ω ·m, much less than the difference calculated at the location of contaminated sand. Moreover, the similar contour shapes of the red and blue solid lines suggest that, unlike the resistivity difference of contaminated sand, the difference

between the two sandboxes within the red solid lines is mainly influenced by the migration of the oxidation plume. In addition, the average resistivity difference of the unsaturated zone (z>39 cm, above red dashed line) is small compared to that of the saturated zone.

To characterize the resistivity variations in even more detail, Fig. 8 shows the temporal development of the resistivity difference between the two sandboxes at x=30 cm and various z positions (black dashed line in Fig. 7). Based on the observed resistivity differences, we identified four zones: below the contaminated sand (0-20 cm), bottom of the contaminated sand (20-30 cm), top of the contaminated sand (30-42 cm) and above the contaminated sand (42-51 cm). In the zone below the contaminated sand, the resistivity difference is increasing with time (Fig. 8b). The oxidation plume gradually migrates downward in the early stages (before day 55) due to density, which explains the increase of the resistivity difference. The oxidation plume partly consists of ions that are continuously released by the degradation reaction. Therefore, the plume continues to extend to both sides under the effect of concentration differences, resulting in a flat overall change in the later stages of the experiment. This is consistent with the fact that the hydrochemical parameters measured in the monitoring tubes are low until day 50-60. The resistivity difference of the area with contaminated sand shows two opposite trends. For the bottom part of the contaminated sand, the resistivity difference between the two sandboxes is decreasing with time (from 1062.3 Ω ·m to 972.3 Ω ·m) (Fig. 8b) due to the migration of the oxidation plume. Thus we speculate that, besides

the oxidation plume, the consumption of contaminants and the generation of degradation products are the main reasons for the resistivity difference in this area. With respect to the top part of the contaminated sand, a small amount of persulfate migrates upward under the effect of injection pressure (see day 21 in Fig. 6). As a result, degradation and the corresponding resistivity difference decreases with increasing distance from the injection position, i.e., the resistivity difference decreases with increasing elevation. On the other hand, the increase in resistivity difference at z=38 cm and z=41 cm is the main reason for the increasing trend of the average resistivity difference (Fig. 8b). This is related to the difference in saturation height of the reference sandbox (39.3 cm) and the remediation sandbox (40.1 cm) (Fig. 7). For the unsaturated zone above the contaminated sand, the resistivity difference between the two sandboxes shows a gradual but insignificant increasing trend (slope = 4.16 and $R^2=0.55$). However, it should be noted that this part does not involve diesel contamination or oxidation plume migration, and the average resistivity difference is only $60 \Omega \cdot m$.

Overall, the resistivity differences between the reference and remediation sandboxes are related to changes in concentration of the contaminant, migration of the oxidation plume, and evaporation at the surface. For the contaminated source zone near the injection well, consumption of contaminants, generation of degradation products and migration of the oxidation plume are determining the decrease in resistivity after persulfate injection. For the non-contaminated areas around the source zone, the migration of the oxidation plume is determining the decrease in resistivity. For field-

scale ISCO remediation, it can thus be concluded that resistivity changes in areas with low initial contamination concentration are expected to be mainly related to the migration of the oxidation plume, making it difficult to discern the degradation of contaminants. There are only few studies on ERT monitoring of base-activated persulfate degradation of hydrocarbon-contaminated soils. Taking a similar case as an example, Hatre et al. had conducted geophysical monitoring of in-situ permanganate remediation process of PCE at field scale, speculated that the low resistivity response was due to oxidant, and guessed that the resistivity decrease due to contaminant degradation was estimated to account for only 5-10%

4.3 Effect of oxidation plume on resistivity of contaminated soil

As the diesel concentration and the oxidation plume are the main drivers of the decrease of the resistivity, it is important to understand the relationship between resistivity and contaminant concentration in the presence of the oxidizing plume. The relationships between resistivity and the chemical parameters indicating contamination (TPH and TOC) obtained from reference sandbox are shown in Fig. 9, and the data from remediation sandbox (black solid rectangle) are also shown in the figure. Here, resistivity is the average value within the sampling area. For the reference sandbox, the resistivity is expected to be related to the contaminant concentration based on the sand column experiments and previous studies (Revil et al., 2011; Schwartz et al., 2012; Mao et al., 2016). This is confirmed by Fig. 9, which shows a relationship between resistivity and TPH and TOC of the soil samples (S9-S16 in reference sandbox) with relatively

high explained variance (R^2 =0.94 and 0.97). As expected, resistivity increased with increasing TPH and TOC.

For the remediation sandbox, the relationships between resistivity and the chemical parameters indicating contamination are less pronounced, which reflects the degradation effect of persulfate on diesel contamination. Note that both S1 and S6 are located in the area above the height of oxidation plume migration (z>34 cm), which means that the resistivity is less affected by the plume. The other sampling locations are all below the height of the area affected by the oxidation plume, and the resistivity is lower than expected under the influence of the plume. Accordingly, it is difficult to accurately distinguish the contamination and the oxidation plume based on the resistivity alone. Likewise, resistivity can be influenced by the contaminated source and plume zones in a field survey, but it cannot directly distinguish these zones (e.g., Elis, et al., 2016).

Based on the fitting line calculated from the reference sandbox data, the relationship model between resistivity and TPH without in-situ remediation is shown as follows:

$$\rho'=0.089C_{TPH}+168.4,$$
 (21)

where ρ ' represents the calculated resistivity without in-situ remediation, C_{TPH} is the concentration of TPH, respectively. In this study, the deviation between measured resistivity and calculated resistivity is caused by migration of oxidant plume. Therefore, the influence ratio of oxidant plume (I_O) is:

$$I_O = |\rho' - \rho_{\text{measure}}|/\rho' \cdot 100\%, \tag{22}$$

while the influence ratio of contaminant consumption (I_C) is:

$$I_C = |1 - I_O| \cdot 100\%$$
. (23)

For remediation sandbox, the influence ratio of oxidant and contaminant consumption on resistivity decrease at difference locations are shown in Table 4. Note that the influence ratios of different factor are calculated by average deviation of TPH. For the areas above the height of the persulfate outflow hole, e.g., S1 and S6, the oxidant plume has a smaller effect on resistivity decrease than contaminant consumption. For the contaminated source zone near the injection well, i.e., S2, although the influence of oxidant plume is dominant, contaminant consumption contributes to 25.6% of the resistivity decrease. For area with low or non-contaminated area, the influence of contaminant consumption on resistivity decrease is less than 16%. The ratio calculated based on the relationship between TOC and resistivity is similar to the ratio shown in Table 4.

Although the half-life of persulfate is 10 to 20 days when reacting with hydrocarbon contaminants in water (Watts, 2011), the degradation rate of diesel within soil by base-activated persulfate can vary considerably due to different reaction conditions and contamination types. Specifically, previous studies illustrated that aromatic and short-chain aliphatic hydrocarbons in diesel are more easily degraded by persulfate. In contrast, long-chain aliphatic hydrocarbons are considered to be the least degradable due to limited hydrophobicity and strong sorption on the soil (Siegrist et al., 2011). For

example, Lominchar et al. (2018) reported that dodecane, tetradecane, pentadecane and aromatic hydrocarbons were essentially degraded by base-activated persulfate in the first 4 days, while aliphatic hydrocarbons with carbon numbers above 16 were more recalcitrant, and still present in small amounts at the end of the treatment after 56 days. To obtain contaminant information during persulfate remediation, resistivity measurements should thus be combined with sampling data for comprehensive analysis.

In the field, ERT method has advantages and challenges to dynamically monitor the insitu remediation process of contaminants. On one hand, it utilizes multiple monitoring modes, i.e., surface, cross-borehole, or in a combination of cross-borehole-surface, and is able to delineate the resistivity changes over a wide remediation area, especially the migration range of oxidants plume. This means ERT can quickly identify the area not covered by oxidant for secondary injection, and can improve efficiency while reducing sampling costs. On the other hand, it is difficult to directly distinguish the effects of oxidant plume and contaminant consumption on resistivity decrease, and a comprehensive analysis combined with sampling data is usually required. This study quantified the effect of hydrocarbon removal on resistivity change based on wellcontrolled conditions, e.g., the contribution of contaminant consumption to resistivity change in the source area is 25.6%, while it is less than 16% in the low or noncontaminated area. However, this contribution is related to the soil characteristics, the type and concentration of contaminant and oxidant, thus it may vary in the field or other laboratory conditions.

5. Conclusion

This study directly visualized the remediation of diesel-contaminated soil by baseactivated persulfate using cross-borehole ERT measurements, and evaluated the capability of resistivity measurements for characterizing oxidation plume migration and contaminant degradation. Since the resistivity response is affected by diesel content and the presence of persulfate, two sandbox experiments were conducted to compare the resistivity distribution of diesel-contaminated sand with and without the persulfate remediation system. To support the interpretation of the resistivity measurements, hydrochemical measurements were made periodically. The results indicated that the resistivity was significantly decreased in response to persulfate injection for the remediation sandbox, e.g., from 846 Ω ·m to below 10 Ω ·m for contaminated sand. Natural degradation and contaminant plume migration were not evident for the reference sandbox without persulfate injection. The chemical parameters, i.e., ORP, pH, DO and conductivity, showed a noticeable increase due to the oxidant injection, while the parameters measured in the reference sandbox showed a gentle and slightly downward trend. Moreover, the results of soil and water samples suggested that the hydroxyl and sulfate radicals formed by base-activated persulfate resulted in substantial degradation of diesel, producing a large number of ions that further decreased the resistivity.

Resistivity ratio tomograms allowed to delineate the area affected by oxidation plume

migration. It was observed that the persulfate plume mainly migrated vertically due to density-driven distribution after an initial phase of horizontal flow associated with the high-pressure injection. In addition, the resistivity difference between the contaminated areas of the two sandboxes was related to the change in contaminant concentration and the migration of the oxidation plume. In the contaminated source zone near the injection well, consumption of contaminants, generation of degradation products and migration of the oxidation plume determined the decrease in resistivity after persulfate injection, while in the low or non-contaminated area around the source zone, the oxidation plume was dominant for the decrease in resistivity.

It was found that the resistivity correlates well with the contaminant indicators, i.e., TPH and TOC. However, the resistivity corresponding to contaminated indicators was generally lower than expected in the presence of the oxidation plume. This further illustrates that resistivity changes due to the decrease of contaminant concentrations after degradation are still influenced by the oxidation plume even in the source zone near the injection well. Concretely, for the contaminated source zone near the injection well, contaminant consumption contributes to 25.6% of the resistivity decrease; while for area with low or non-contaminated area, the influence of contaminant consumption on resistivity change is less than 16%.

It is difficult to capture the characteristics of chemical reactions at the pore scale using the ERT method. An extension of ERT is the induced polarization (IP) method, which is more sensitive to properties at the pore scale. Future research should thus additionally consider the IP response during ISCO remediation, e.g., to characterize chemical reactions of the diesel degradation process. It is necessary to design the periodic contaminant concentration tests for direct comparison of IP parameter changes with degradation processes. Nevertheless, the ERT monitoring results presented above for diesel remediation clearly show resistivity responses that are related to the effects of oxidation plume migration and changes in contaminant concentration, which has not been previously reported for the monitoring of the persulfate remediation system.

6. Acknowledge

The corresponding author acknowledges the support from the National Science Foundation (42177056) and Shandong National Science Foundation (ZR2019MEE109).

References

- Alpaslan, N. 2021. Determination of borehole locations and saline-water intrusion for groundwater in Central Anatolia Region, Turkey using electrical tomography (ERT) method. Environmental Earth Sciences, 80, 810. https://doi.org/10.1007/s12665-021-10117-7.
- Arato, A., Wehrer, M., Biró, B., Godio, A., 2014. Integration of geophysical, geochemical and microbiological data for a comprehensive small-scale characterization of an aged LNAPL-contaminated site. Environmental Science and Pollution Research, 21, 8948–8963. https://doi.org/10.1007/s11356-013-2171-2.
- Atekwana, E.A., Atekwana, E.A., 2010. Geophysical signatures of microbial activity at hydrocarbon contaminated sites: a review. Surveys in Geophysics, 31,247–283. https://doi.org/10.1007/s10712-009-9089-8.
- Binley, A., Slater, L.D., 2020. Resistivity and Induced Polarization. In Resistivity and Induced Polarization: Theory and Applications to the Near-Surface Earth (p. I). Cambridge: Cambridge University Press.
- Chang, Y.C., Peng, Y.P., Chen, K.F., Chen, T.Y., Tang, C.T., 2022. The effect of different in situ chemical oxidation (ISCO) technologies on the survival of indigenous microbes and the remediation of petroleum hydrocarbon-contaminated soil. Process Safety and Environmental Protection, 163, 105-115. https://doi.org/10.1016/j.psep.2022.05.019.
- China Geological Survey, 2014. Geological survey and evaluation standards for Soil and Groundwater in contaminated (DD sites 2014-06), http://www.cgs.gov.cn/upload/201501/20150105/20150327112909776.pdf Coscia, I., Greenhalgh, S.A., Linde, N., Doetsch, J., Marescot, L., Günther, T., Vogt, T., Green, A.G., 2011. 3D crosshole ERT for aquifer characterization and monitoring of Geophysics, 76 G49-G59. infiltrating river water. (2),https://doi.org/10.1190/1.3553003.
- Cronk, G., 2008. Case Study Comparison of Multiple Activation Methods for Sodium Persulfate ISCO Treatment. Presentation at the Battelle 6 th International Conference on Remediation of Chlorinated and Recalcitrant Compounds, May 19-22.

- Dahlin, T., Zhou, B., 2006. Multiple-gradient array measurements for multichannel 2D resistivity imaging. Near Surface Geophysics, 4, 113–123. https://doi.org/10.3997/1873-0604.2005037.
- Deng, Y.P., Shi, X.Q., Xu, H.X., Sun, Y.Y., Wu, J.C., Revil, A., 2017. Quantitative assessment of electrical resistivity tomography for monitoring DNAPLs migration Comparison with high-resolution light transmission visualization in laboratory sandbox. Journal of Hydrology, 544, 254-266. https://doi.org/10.1016/j.jhydrol.2016.11.036.
- Elis, V.R., Ustra, A.T., Hidalgo-Gato, M.C., Pejon, O.J., Hiodo, F.Y., 2016. Application of induced polarization and resistivity to the environmental investigation of an old waste disposal area. Environmental Earth Sciences, 75, 1338. https://doi.org/10.1007/s12665-016-6157-5.
- Flores Orozco, A., Velimirovic, M., Tosco, T., Kemna, A., Sapion, H., Klaas, N., Sethi, R., Bastiaens, L., 2015. Monitoring the injection of microscale zerovalent iron particles for groundwater remediation by means of complex electrical conductivity imaging. Environmental Science & Technology, 49(9), 5593-5600. https://doi.org/10.1021/acs.est.5b00208.
- Furman, O.S., Teel, A.L., Watts, R.J., 2010. Mechanism of Base Activation of Persulfate. Environmental Science & Technology, 44(16), 6423-6428. https://doi.org/10.1021/es1013714.
- Gad, S.C., 2005. Diesel Fuel. In: Wexler, P., Encyclopedia of Toxicology (Second Edition). Elsevier, 19-22. https://doi.org/10.1016/B0-12-369400-0/00320-3.
- Halihan, T., Sefa, V., Sale, T., Lyverse, M., 2017. Mechanism for detecting NAPL using electrical resistivity imaging. Journal of Contaminant Hydrology, 205, 57-69. https://doi.org/10.1016/j.jconhyd.2017.08.007.
- Harte, P.T., Smith, T.E., Williams, J.H., Degnan, J.R., 2012. Time series geophysical monitoring of permanganate injections and in situ chemical oxidation of PCE, OU1 area, Savage Superfund Site, Milford, NH, USA. Journal of Contaminant Hydrology, 132, 58-74. https://doi.org/10.1016/j.jconhyd.2012.01.008.

- Hayyan, M., Hashim, M.A., AlNashef, I.M., 2016. Superoxide ion: generation and chemical implications. Chemical Review. 116, 3029–3085. https://doi.org/10.1021/acs.chemrev.5b00407.
- He, L.P., Tong, J.H., Yang, Y.Q., Wu, J.X., Li, L.Q., Wei, Z.H., Long, W., Pang, J.L., Shi, J.Y., 2022. Overestimate of remediation efficiency due to residual sodium persulfate in PAHs contaminated soil and a solution. Journal of Environmental Sciences, 113, 242-250. https://doi.org/10.1016/j.jes.2021.06.004.
- Hewelke, E., Szatyłowicz, J., Hewelke, P., Gnatowski, T., Aghalarov, R., 2018. The Impact of diesel oil pollution on the hydrophobicity and CO₂ efflux of forest soils. Water, Air, & Soil Pollution, 229, 51. https://doi.org/10.1007/s11270-018-3720-6.
- Huang, K.C., Couttenye, R.A. and Hoag, G.E., 2002. Kinetics of heat-assisted persulfate oxidation of methyl tert-butyl ether (MTBE). Chemosphere, 49(4), 413-420. https://doi.org/10.1016/S0045-6535(02)00330-2.
- Huling, S. G. and Pivetz, B. E. 2006. In-situ chemical oxidation, Cincinnati, Ohio: United States Environmental Protection Agency. EPA/600/R-06/072. https://clu-in.org/download/contaminantfocus/pcb/ISCO-600R06072.pdf.
- Imron, M.F., Kurniawan, S.B., Ismail, N., Abdullah, S.R.S., Future challenges in diesel biodegradation by bacteria isolates: A review. Journal of Cleaner Production, 251, 119716. https://doi.org/10.1016/j.jclepro.2019.119716.
- Kang, X.Y., Shi, X.Q., Deng, Y.P., Revil, A., Xu, H.X., Wu, J.C., 2018. Coupled hydrogeophysical inversion of DNAPL source zone architecture and permeability field in a 3D heterogeneous sandbox by assimilation time-lapse cross-borehole electrical resistivity data via ensemble Kalman filtering. Journal of Hydrology, 567, 149-164. https://doi.org/10.1016/j.jhydrol.2018.10.019.
- Karthick, A., Roy, B., Chattopadhyay, P., 2019. A review on the application of chemical surfactant and surfactant foam for remediation of petroleum oil contaminated soil.
 Journal of Environmental Management, 243, 187-205.
 https://doi.org/10.1016/j.jenvman.2019.04.092.
- Kemna, A., Kulessa, B., Vereecken, H., 2002. Imaging and characterization of subsurface solute transport using electrical resistivity tomography (ERT) and

- equivalent transport models. Journal of Hydrology, 267 (3–4), 125–146. https://doi.org/10.1016/S0022-1694(02)00145-2.
- Khudur, L.S., Shahsavari, E., Miranda, A.F., Morrison, P.D., Nugegoda, D., Ball, A.S., 2015. Evaluating the efficacy of bioremediating a diesel-contaminated soil using ecotoxicological and bacterial community indices. Environmental Science and Pollution Research, 22, 14809-14819. https://doi.org/10.1007/s11356-015-4624-2.
- Lekmine, G., Auradou, H., Pessel, M., Rayner, J.L., 2017. Quantification of tracer plume transport parameters in 2D saturated porous media by cross-borehole ERT imaging. Journal of Applied Geophysics, 139, 291-305. http://dx.doi.org/10.1016/j.jappgeo.2017.02.024.
- Lesmes, D. P., Frye, K. M., 2001. Influence of pore fluid chemistry on the complex conductivity and induced polarization responses of Berea sandstone. Journal of Geophysical Research, 106(B3), 4079–4090. https://doi.org/10.1029/2000JB900392.
- Liang, C., Guo, Y.Y., 2012. Remediation of Diesel-Contaminated Soils Using Persulfate Under Alkaline Condition. Water, Air, & Soil Pollution. 223, 4605–4614. https://doi.org/10.1007/s11270-012-1221-6.
- Liang, C.J., Lee, I.L., 2008. In situ iron activated persulfate oxidative fluid sparging treatment of TCE contamination A proof of concept study. Journal of Contaminant Hydrology, 100(3-4), 91-100. https://doi.org/10.1016/j.jconhyd.2008.05.012.
- Li, Y.T., Li, D., Lai, L.J., Li, Y.H., 2020. Remediation of petroleum hydrocarbon contaminated soil by using activated persulfate with ultrasound and ultrasound/Fe. Chemosphere, 238, 124657. https://doi.org/10.1016/j.chemosphere.2019.124657.
- Liu, H.Z., Bruton, T.A., Li, W., Buren, J.V., Prasse, C., Doyle, F.M., Sedlak, D.L., 2016.

 Oxidation of Benzene by Persulfate in the Presence of Fe(III)- and Mn(IV)Containing Oxides: Stoichiometric Efficiency and Transformation Products.

 Environmental Science & Technology, 50(2), 890-898.

 https://doi.org/10.1021/acs.est.5b04815.
- Loke, M.H., Wilkinson, P.B., Chambers, J.E., Uhlemann, S.S., Sorensen, J.P.R., 2015. Optimized arrays for 2-D resistivity survey lines with a large number of electrodes.

- Journal of Applied Geophysics, 112, 136-146. https://doi.org/10.1016/j.jappgeo.2014.11.011.
- Lominchar, M.A., Santos, A., de Miguel, E., Romero, A., 2018. Remediation of aged diesel contaminated soil by alkaline activated persulfate. Science of the Total Environment, 622-623, 41-48. https://doi.org/10.1016/j.scitotenv.2017.11.263.
- Mao, D.Q., Lu, L., Revil, A., Zuo, Y., Hinton, J., Ren, Z.J., 2016. Geophysical Monitoring of Hydrocarbon-Contaminated Soils Remediated with a Bioelectrochemical System. Environmental Science & Technology, 50(15), 8205–8213. https://doi.org/10.1021/acs.est.6b00535.
- Mao, D.Q., Revil, A., Hort, R.D., Munakata-Marr, J., Atekwana, E.A., Kulessa, B., 2015. Resistivity and self-potential tomography applied to groundwater remediation and contaminant plumes: Sandbox and field experiments. Journal of Hydrology, 530, 1-14. http://dx.doi.org/10.1016/j.jhydrol.2015.09.031.
- Mellage, A., Holmes, A.B., Linley, S., Vallée, L., Rezanezhad, F., Thomson, N., Gu, F. and Cappellen, P.V., 2018. Sensing coated iron-oxide nanoparticles with spectral induced polarization (SIP): Experiments in natural sand packed flow-through columns. Environmental Science & Technology, 52 (24), 14256-14265. http://doi.org/10.1021/acs.est.8b03686.
- Müller, K., Vanderborght, J., Englert, A., Kemna, A., Huisman, J.A., Rings, J., Vereecken, H., 2010. Imaging and characterization of solute transport during two tracer tests in a shallow aquifer using electrical resistivity tomography and multilevel groundwater samplers. Water Resource Research, 46, W03502. http://doi.org/10.1029/2008WR007595.
- Niu, Q.F., Revil, A., Saldian, M., 2016. Salinity dependence of the complex surface conductivity of the Portland sandstone. Geophysics, 81(2), D125–D140. https://doi.org/10.1190/geo2015-0426.1.
- Pinedo, J., Ibáñez, R., Lijzen, J, Irabien, A., 2013. Assessment of soil pollution based on total petroleum hydrocarbons and individual oil substances. Journal of Environmental Management, 130, 72-79. https://doi.org/10.1016/j.jenvman.2013.08.048.

- Revil, A., Schmutz, M., Batzle, M.L., 2011. Influence of oil wettability upon spectral induced polarization of oil-bearing sands. Geophysics, 76(5), A31-A36. https://doi.org/10.1190/GEO2011-0006.1.
- Schmutz, M., Revil, A., Vaudelet, P., Batzle, M., Viñao, P. F., Werkema, D. D., 2010. Influence of oil saturation upon spectral induced polarization of oil-bearing sands. Geophysical Journal International, 183(1), 211–224. https://doi.org/10.1111/j.1365-246X.2010.04751.x.
- Schwartz, N., Huisman, J. A., Furman, A., 2012. The effect of NAPL on the electrical properties of unsaturated porous media. Geophysical Journal International, 188(3), 1007-1011. https://doi.org/10.1111/j.1365-246X.2011.05332.x.
- Seferou, P., Soupios, P., Kourgialas, N.N., Dokou, Z., Karatzas, G.P., Candasayar, E., Papadopoulos, N., Dimitriou, V., Sarris, A., and Sauter, M., 2013. Olive-oil mill wastewater transport under unsaturated and saturated laboratory conditions using the geoelectrical resistivity tomography method and the FEFLOW model. Hydrogeology Journal, 21, 1219–1234. https://doi.org/10.1007/s10040-013-0996-x.
- Sentenac, P., Hogson, T., Keenan, H., Kulessa, B., 2015. Small scale monitoring of a bioremediation barrier using miniature electrical resistivity tomography. Journal of Applied Geophysics, 115, 24-31. https://doi.org/10.1016/j.jappgeo.2014.11.006.
- Serrano, A., Gallego, M., González, J.L., Tejada, M., 2008. Natural attenuation of diesel aliphatic hydrocarbons in contaminated agricultural soil. Environmental Pollution, 151(3), 494-502. https://doi.org/10.1016/j.envpol.2007.04.015.
- Shang, Z., Xu, P., Yue, H. Feng, D.Y., Zhu, T.H., Li, X.X., 2022. Remediation of diesel-contaminated soil by alkoxyethanol aqueous two-phase system. Environmental Science and Pollution Research, 29, 25810–25823. https://doi.org/10.1007/s11356-021-17836-1.
- Siegrist, R.L., Crimi, M., Simpkin, T.J., 2011. In Situ Chemical Oxidation for Groundwater Remediation. Springer-Verlag New York, New York.
- Slater, L., Binley, A.M., Daily, W., Johnson, R., 2000. Cross-hole electrical imaging of a controlled saline tracer injection. Journal of Applied Geophysics, 44(2–3), 85–102. https://doi.org/10.1016/S0926-9851(00)00002-1.

- Waldemer. R.H., Tratnyek, P.G., Johnson, R.L., Nurmi, J.T., 2007. Oxidation of Chlorinated Ethenes by Heat-Activated Persulfate: Kinetics and Products. Environmental Science & Technology, 41, 1010-1015. https://doi.org/10.1021/es062237m.
- Watts, R.J., 2011. Enhanced Reactant-Contaminant Contact through the Use of Persulfate In Situ Chemical Oxidation (ISCO). http://doi.org/10.21236/ada579945.
- Wu, Y.Y, 2021. Bicarbonate use and carbon dioxide concentrating mechanisms in photosynthetic organisms. Acta Geochimica, 40, 846–853. https://doi.org/10.1007/s11631-021-00488-w.
- Wu, Y.X., Hubbard, S., Wellman, D., 2012. Geophysical Monitoring of Foam Used to Deliver Remediation Treatments within the Vadose Zone. Vadose Zone Journal, 11(4), 280-288. https://doi.org/10.2136/vzj2011.0160.
- Xia, T., Dong, Y., Mao, D. and Meng, J., 2021. Delineation of LNAPL contaminant plumes at a former perfumery plant using electrical resistivity tomography. Hydrogeology Journal, 29(3), 1189-1201. http://doi.org/10.1007/s10040-021-02311-5.
- Yen, C.H., Chen, K.F., Kao, C.M., Liang, S.H., Chen, T.Y., 2011. Application of persulfate to remediate petroleum hydrocarbon-contaminated soil: Feasibility and comparison with common oxidants. Journal of Hazardous Materials, 186(2-3), 2097-2102. https://doi.org/10.1016/j.jhazmat.2010.12.129.
- Zhao, D., Liao, X.Y., Yan, X.L., Huling, S.G., Chai, T.Y., Tao, H., 2013. Effect and mechanism of persulfate activated by different methods for PAHs removal in soil. Journal of Hazardous Materials, 254-255, 228-235. https://doi.org/10.1016/j.jhazmat.2013.03.056.

Table 1 Summary statistics of the sandbox experiment.

Soil volume	Pore volume	Volume of persulfate and base	Contaminated soil volume	Diesel content	Mass ratio of
(L)	(L)	$(Na_2S_2O_8+NaOH, mL)$	(L)	(g/kg)	persulfate and diesel
30	12.3	250 + 250	1.76	105.9	0.13

Table 2: Values of the phase and the modulus of the resistivity at the peak of the relaxation for sand saturated by the non-wetting oil.

Water saturation Sw (-)	Diesel content (g/kg)	Phase (mrad)	Resistivity (Ω·m)		
1	0.0	2.36	82.6		
0.95	10.6	3.26	139.4		
0.7	63.5	4.96	473.5		
0.5	105.9	6.60	745.2		

Table 3 Concentrations of major contaminated indicators measured in soil and water samples.

								Soil s	samples							
Indicators				TOC	(g/kg)							TF	PH (g/kg)			
Remediation	S1	S2	S3	S4	S5	S6	S7	S8	S1	S2	S3	S4	S5	S6	S7	S8
sandbox	9.5	1.73	1.4	4.21	2.17	0.74	0.82	0.26	5.94	1.67	0.153	2.54	0.538	0.2	0.126	0.12
Reference	S9	S10	S11	S12	S13	S14	S15	S16	S9	S10	S11	S12	S13	S14	S15	S16
sandbox	36.1	30.2	3.03	7.06	3.77	0.6	0.84	0.28	33.8	27.4	1.97	5.56	2.94	0.587	1.89	0.561
								Water	samples							
Indicators		Petroleum (mg/L) COD (mg/L)					SO ₄ ²⁻ (mg/L)				HCO ₃ - (mg/L)					
Remediation	V	V1	V	V2	W	/1	1	W2	•	W1	W	/2	V	V1	V	V2
sandbox	0.	91	1.	00	2	9		14	3	240	32	30	8	27	7	59
Reference	V	V3	V	V4	W	/3	•	W4	•	W3	W	/4	V	V3	V	V4

TOC: Total Organic Carbon; TPH: Total Petroleum Hydrocarbon; COD: Chemical Oxygen Demand.

126

sandbox

2.32

2.45

153

17.4

10.6

207

201

Table 4 Influence ratio of oxidant plume and contaminant consumption on resistivity decrease at difference locations

Sampling location	Measured	ТРН		Influence ratio of	Influence ratio of contaminant consumption		
	resistivity	Calculated resistivity	Deviation	oxidant plume			
	$(\Omega{\cdot}m)$	$(\Omega{\cdot}m)$	(%)	(%)	(%)		
S1	341.3	697.1	51.1	51.1	48.9		
S2	81.3	317.0	74.4	74.4	25.6		
S3	26.6	182.0	85.4	85.4	14.6		
S4	61.5	394.5	84.4	84.4	15.6		
S5	31.8	216.3	85.2	85.2	14.8		
S6	137.1	186.2	26.4	26.4	73.6		
S7	27.2	179.6	85.0	85.0	15.0		
S8	25.3	179.1	86.0	86.0	14.0		

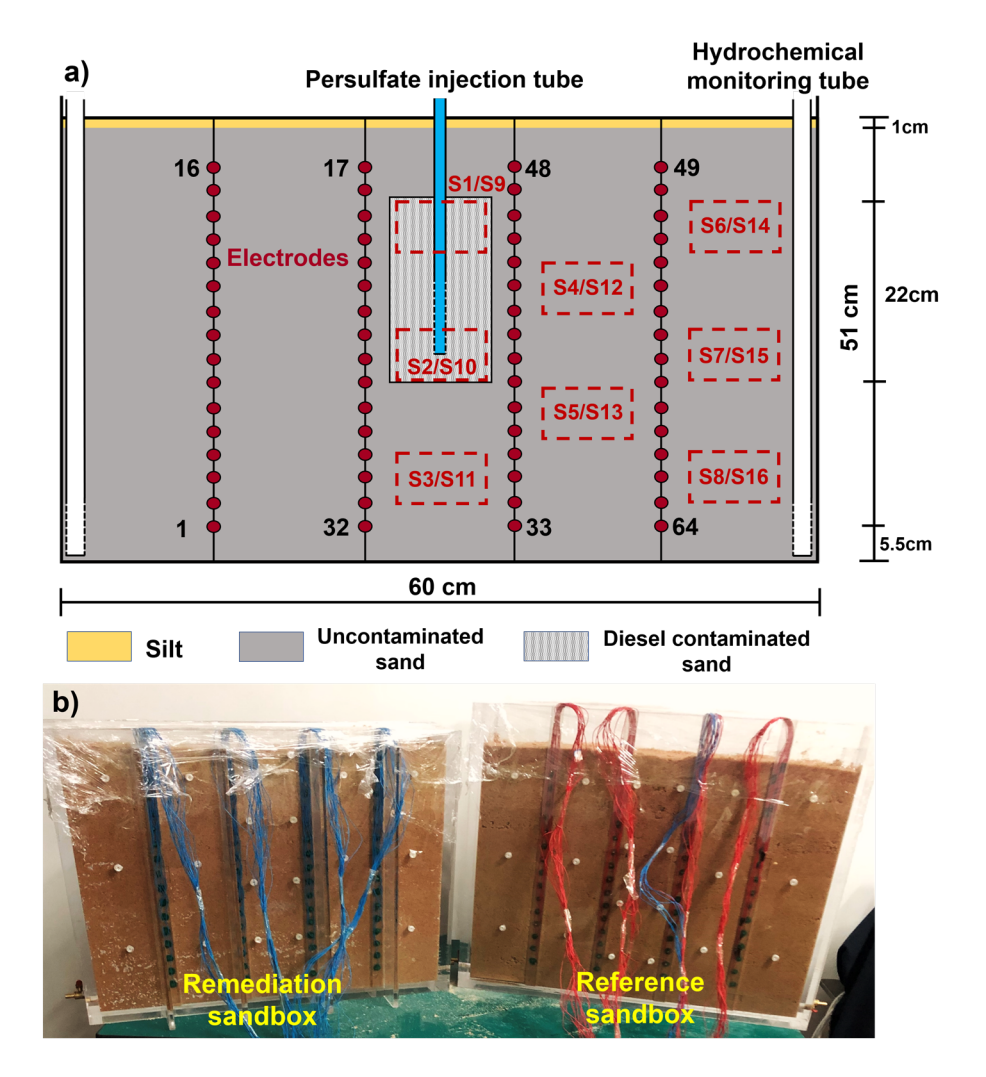


Fig. 1 Sandbox configuration. (a) Front view (51 cm high × 60 cm long× 10 cm thick) and (b) photograph of the sandbox. The upper part was covered with 1cm of silt. A total of 16*4 non-polarizable electrodes (red dots) were attached on the side wall of the sandbox. The white rectangles on the left and right sides indicated the hydrochemical monitoring and sampling tubes. Persulfate was injected at the bottom of the blue rectangle. Soil was sampled at 8 sites (red dashed rectangles) and water was taken at sampling tubes.

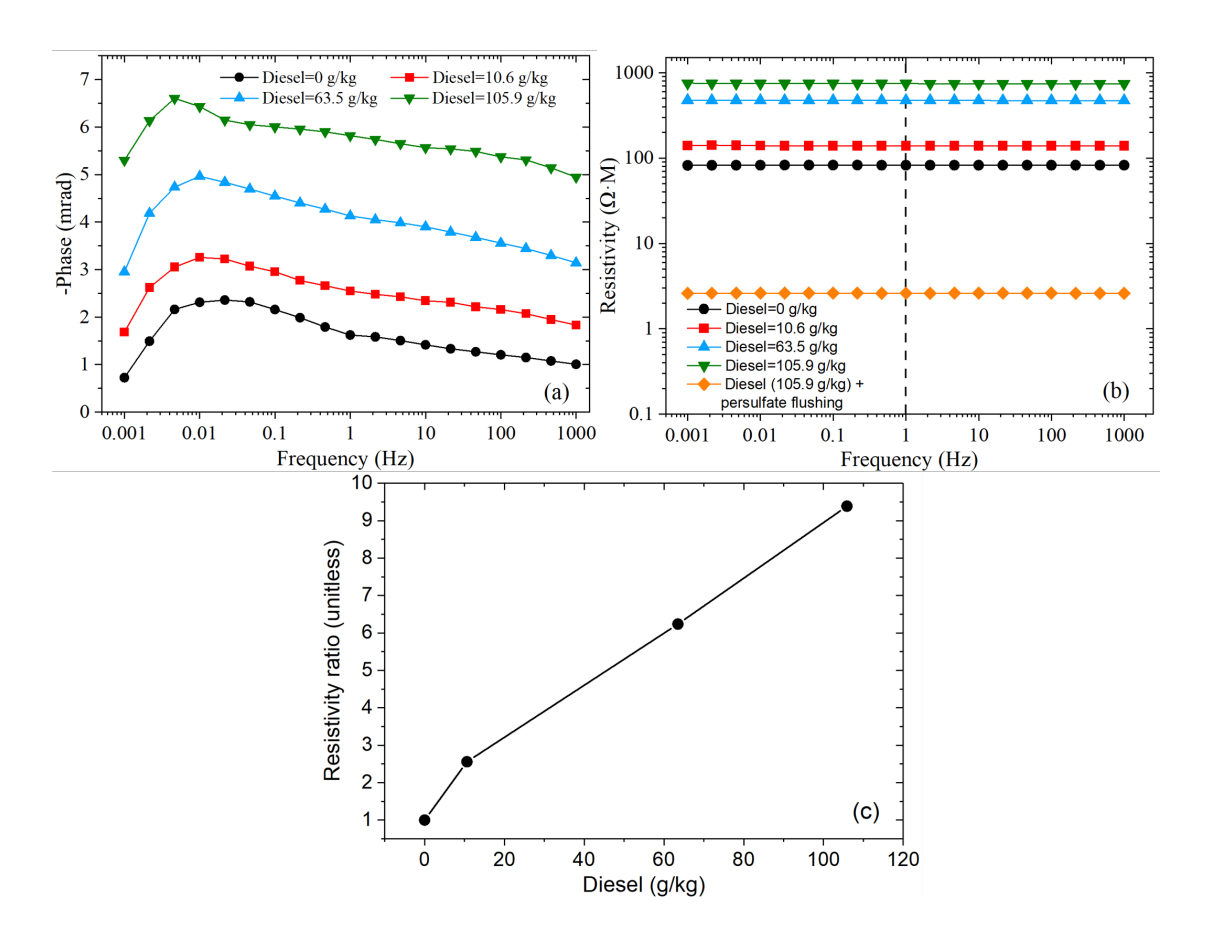


Fig. 2 Results of complex resistivity measurements. (a) Phase and (b) resistivity (ρ) of the complex resistivity for different diesel content. (c) Resistivity ratio ρ/ρ_0 increase with increasing diesel concentration. The solid dots show the resistivity at 1 Hz with different diesel content, and ρ_0 denotes the resistivity of clean sand.

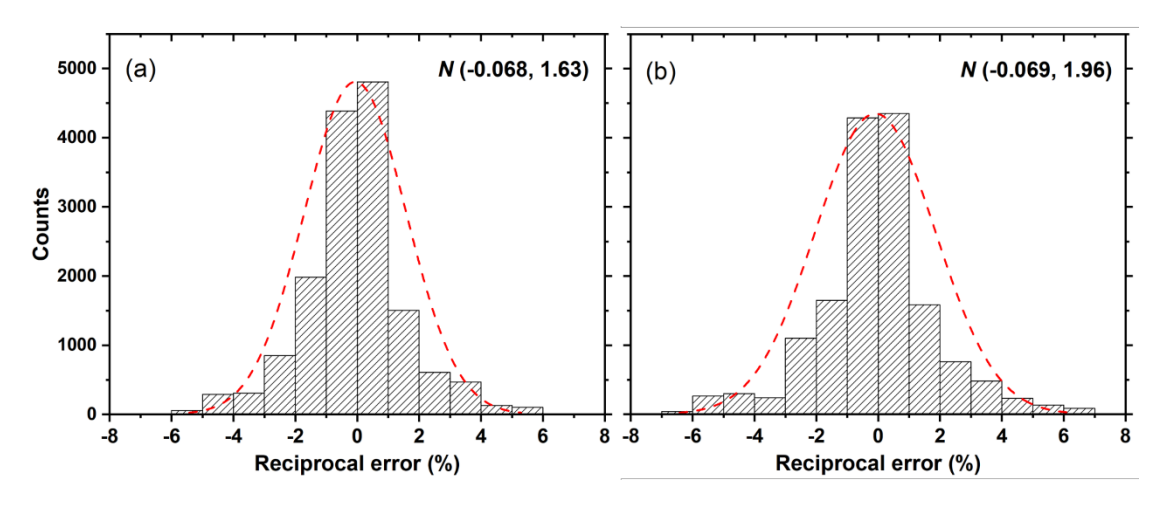


Fig. 3 Reciprocal errors of all datasets taken in (a) reference sandbox and (b) remediation sandbox.

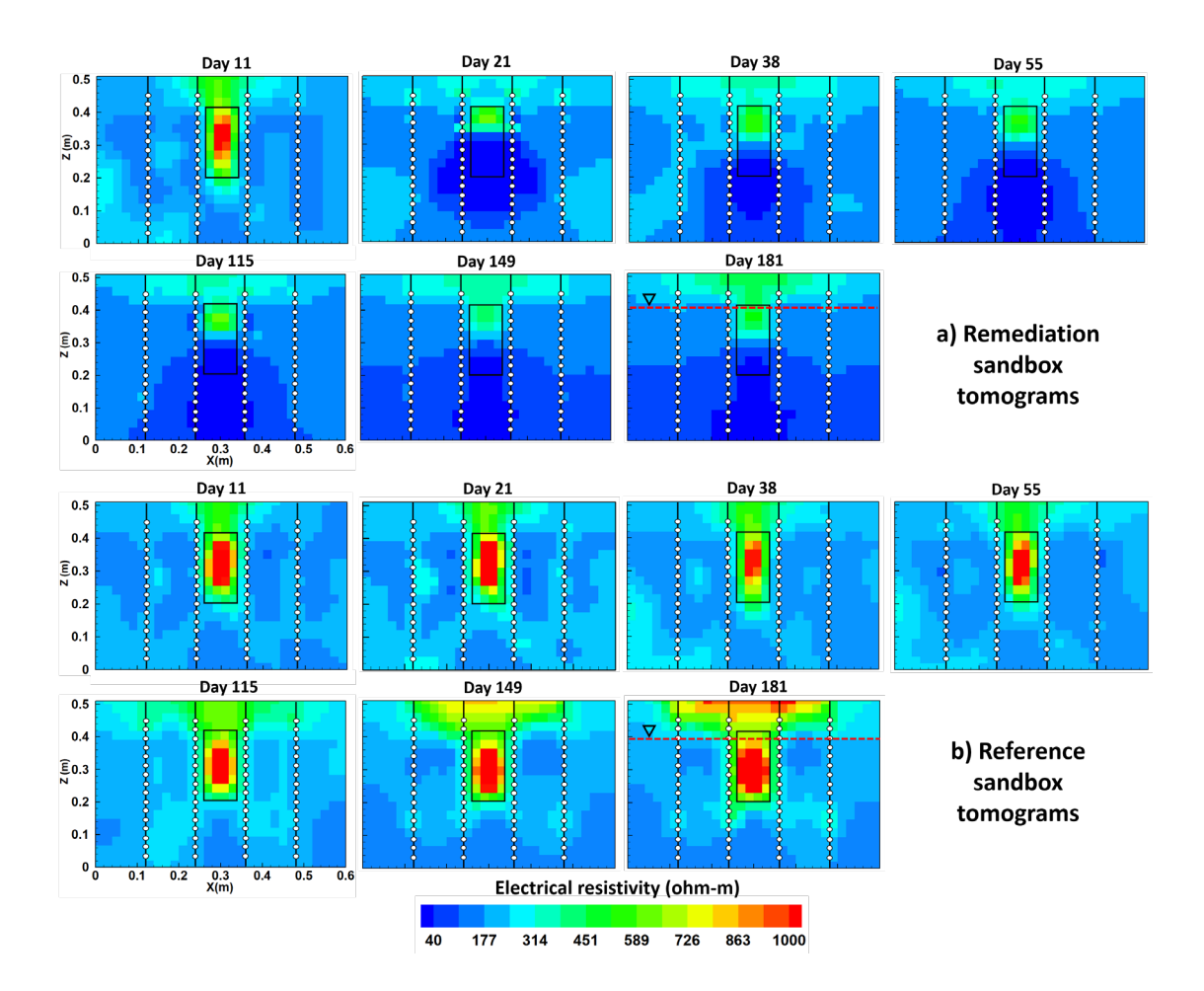


Fig. 4 Geophysical monitoring tomograms. (a) Resistivity tomograms of remediation sandbox. Red color (> 0.45 m) on top of remediation sandbox represents the resistivity response of unsaturated zone. (b) Resistivity tomograms of reference sandbox. The locations of electrodes and contaminated sand are marked in white solid circles and black rectangle. The red dashed line represents the water table.

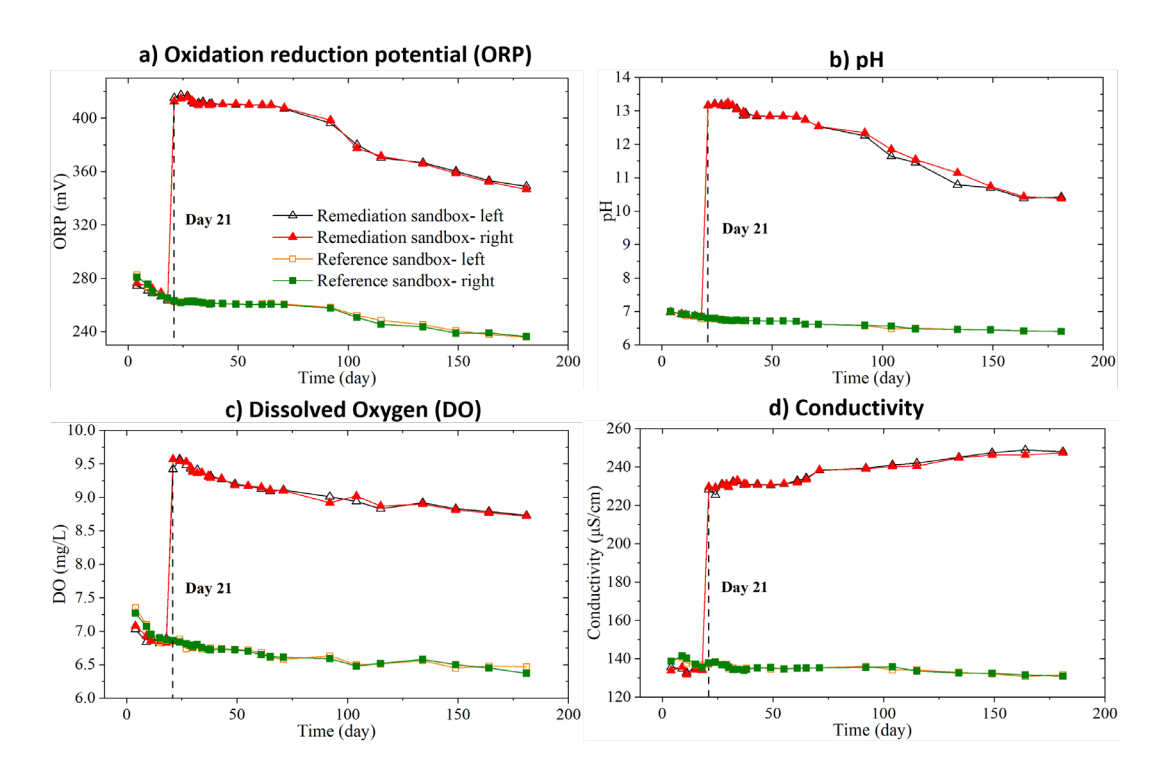


Fig. 5 Plots of (a) ORP, (b) pH, (c) DO and (d) conductivity measured on the left and right sides of two sandboxes. Base-activated persulfate is injected on day 21 and all indicators measured in remediation sandbox represent a noticeable increase after injection.

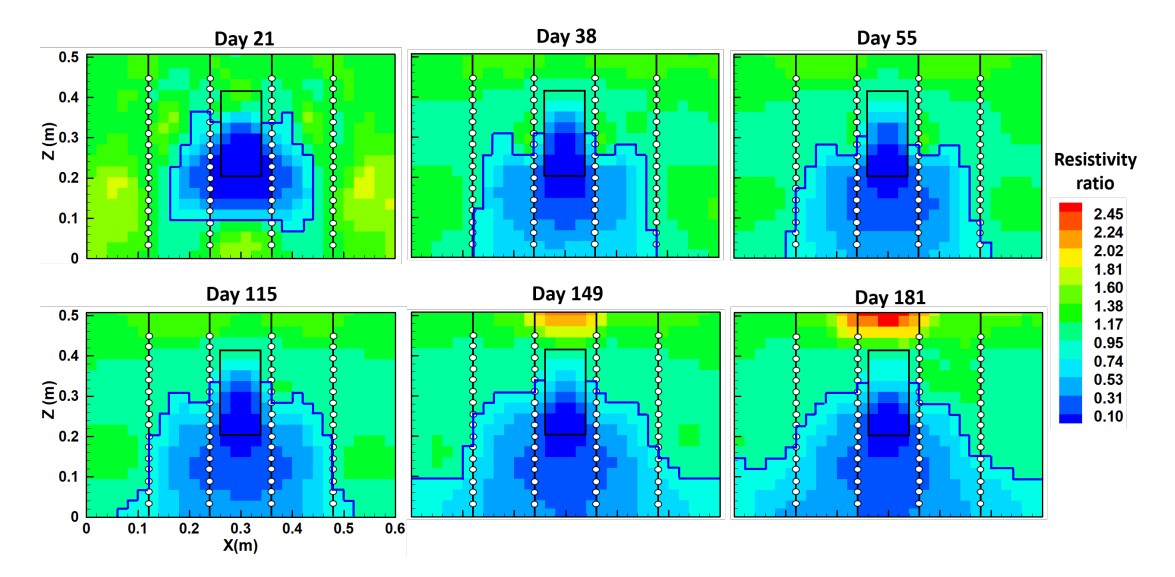


Fig. 6 Resistivity ratio tomograms with respect to the first resistivity tomogram taken at day 11. Blue solid lines (<0.95) represent the influence range of persulfate migration.

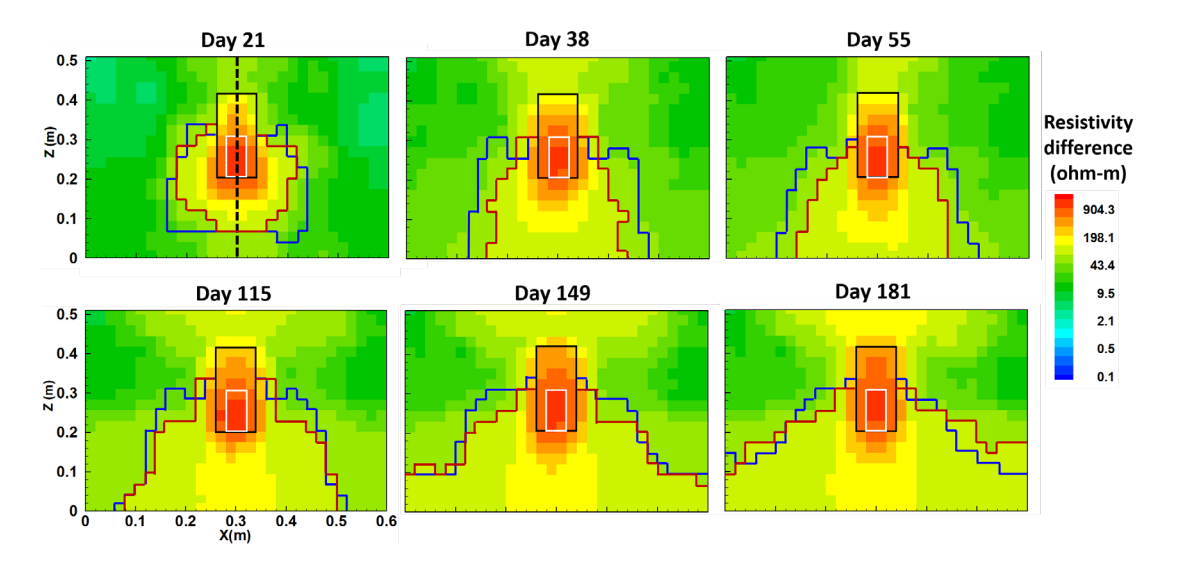


Fig. 7 Resistivity difference tomograms between reference and remediation sandbox.

The central black rectangle indicates the location of contaminated sand and white solid rectangle indicate the persulfate injection location with resistivity difference >600 Ω ·m. The red solid lines indicate the area with resistivity difference >80 Ω ·m, while the area within blue solid lines indicate the zone of resistivity ratio <0.95 in Fig. 5, representing the affected area of oxidation plume.

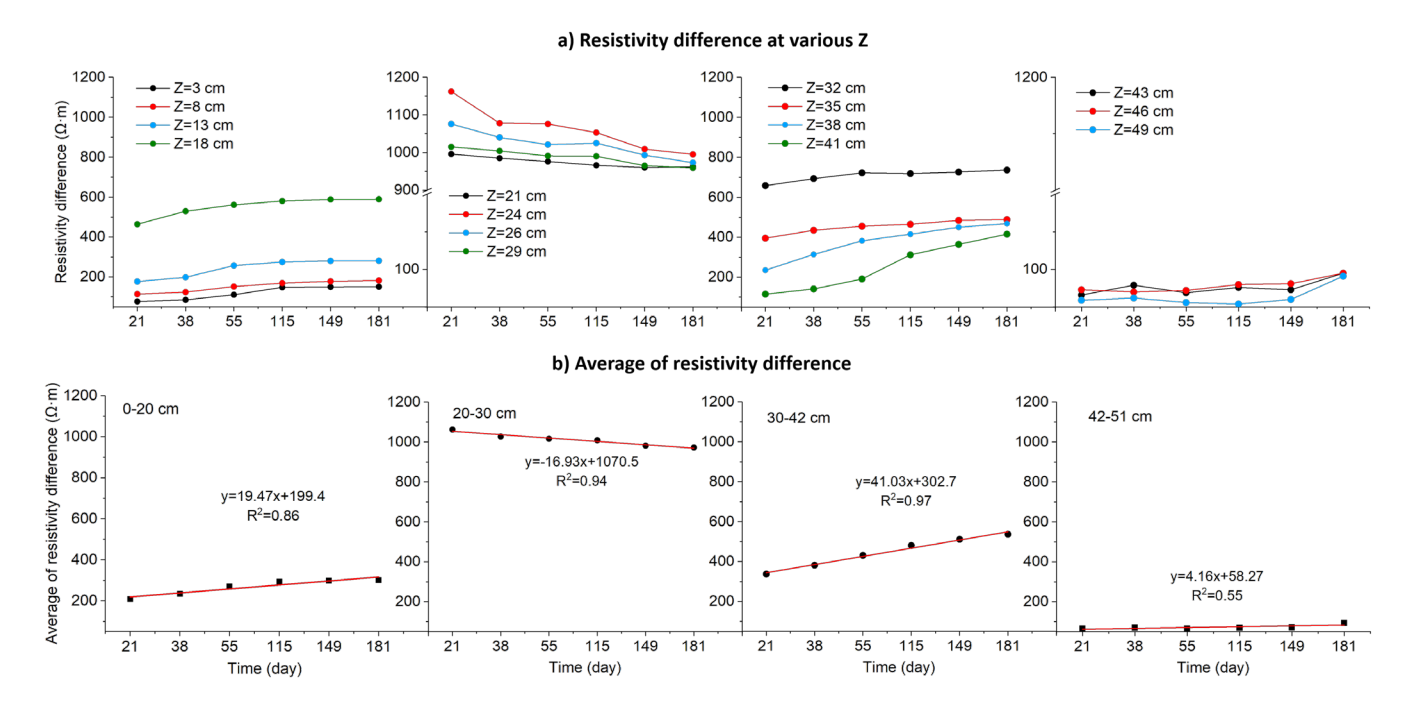


Fig. 8 Time-series of resistivity difference between reference sandbox and remediation sandbox at x=30 cm. (a) Resistivity difference at various z. (b) Average of resistivity difference.

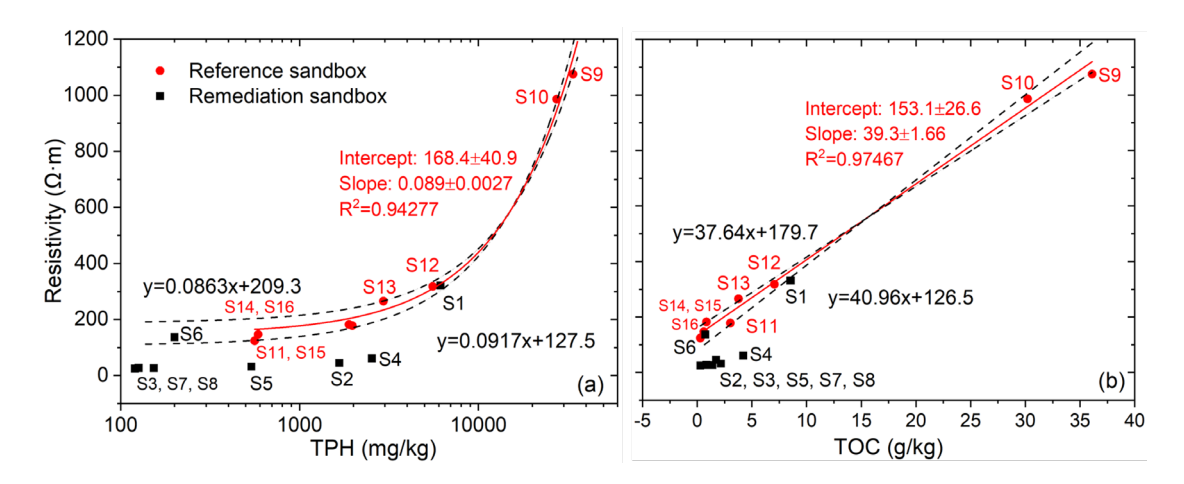


Fig. 9 Relationship between resistivity and (a) TPH, (b) TOC obtained from reference sandbox, and the data from remediation sandbox are also shown in the figure. The solid red line is a linear fitting line for the resistivity and concentration data in the reference sand box. The two dashed lines indicate the confidence intervals of the fitting line, and data measured in the reference sandbox are within the confidence interval. Note that the relationship between resistivity and TPH is presented in semi-log coordinates.